Nanoscale

Accepted Manuscript

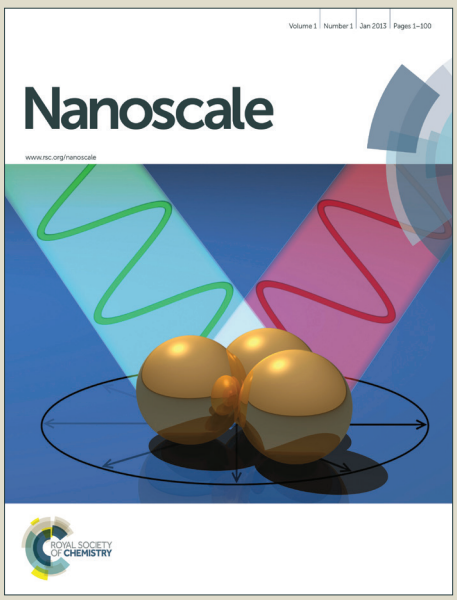

ROYAL SOCIETY OF CHEMISTRY

www.rsc.org/nanoscale

Macroporous Carbon Decorated with Dendritic Platinum Nanoparticles: One-Step Synthesis and Electrocatalytic Properties

Xueqing Yu,[a,b] Yufan Zhang,[b] Liping Guo[b] and Liang Wang[a,*]

[a] State Key Laboratory of Electroanalytical Chemistry, Changchun Institute of Applied Chemistry, Chinese Academy of Sciences, Changchun, Jilin 130022, PR China

[b] Faculty of Chemistry, Northeast Normal University, Changchun, Jilin 130024, PR China

*** Corresponding Author**

E-mail: wangliang@ciac.ac.cn; Tel: +86-431-85262570

Abstract

Macroporous carbon (MPC) with high pore accessibility and electrical conductivity is of great interest electrochemical platform. The development of a simple and efficient route to direct synthesis of dendritic platinum nanoparticles (DPNs) decorated MPC (DPNs/MPC) is an interesting challenge, which is highly valuable for electrocatalytic applications. In this study, we propose a very simple route for one-step synthesis of DPNs/MPC in aqueous solution at room temperature without the need for any of seed and surfactant to direct the dendritic growth of Pt nanoparticles, which is performed by simply mixing aqueous solution of K_2PtCl_4 with MPC and formic acid. As-prepared DPNs/MPC shows high electrocatalytic activities toward the oxidation of methanol and glucose.

1. Introduction

Design and synthesis of platinum (Pt) nanostructures are of great technological interest for the development of catalytic and sensor materials.[1-2] In fuel cells, Pt nanostructures is one of the key electrocatalysts to catalyze oxidation of small organic fuels at the anode and oxygen reaction reduction at the cathode. Pt nanoparticles have also been extensively used for fabricating electrochemical sensing platforms for detection of dopamine,[3] uric acid,[4] H_2O_2,[5] glucose,[6,7] and trinitrotoluene,[8] etc., owing to their intrinsic electrocatalytic properties. Up to date, extensive effort has been devoted to improve the Pt utilization efficiency and enhance its catalytic performance. Rational design of Pt nanostructures with controlled shape and size is a general way to achieve these goals. Thus, Pt nanostructures with various shapes, such as nanosheets, nanocages, nanocubes, etc., [9-17] have been successfully prepared via template-, seed-, and surfactant-directed strategies. Among various Pt nanostructures, dendritic platinum nanoparticles (DPNs) with porous structure and large surface area have stimulated extensive interests. In recent significant achievements, DPNs were successfully synthesized via a seeded growth strategy using tetrahedral Pt nanocrystals as seeds,[12] and via a surfactant-mediated route using triblock copolymer (Pluronic F127) as surfactant,[13] respectively. To date, it remains an interesting challenge to develop a seed- and surfactant-free route to direct synthesis of DPNs.

In comparison with unsupported DPNs, supported DPNs with spatial and local separation on supporter are not susceptible to particle agglomeration, favoring high catalytic performance and long-term stability in catalytic reaction. Suitable supporter

for noble metallic nanoparticles is a critical component for fabricating active, robust and low-cost catalysts. Carbon-based materials are widely used supporters, mainly including carbon nanospheres,[18] carbon nanotubes,[19] graphene oxide,[20] mesoporous carbon materials,[21] etc. In particular, macroporous carbon (MPC) with high pore accessibility and electrical conductivity, which has been widely used as electrochemical platform, is a highly interesting supporter for noble metallic nanocatalysts.[22-25] To the best of our knowledge, there have not been reports on one-step synthesis of DPNs supported on MPC which is highly desired for electrocatalytic applications.

Inspired by this interesting challenge, here we newly developed a one-step route to direct synthesis of DPNs decorated MPC (DPNs/MPC) in aqueous solution at room temperature, which was performed by simply mixing aqueous solution of K_2PtCl_4 with MPC and formic acid. The advantages of the developed route to fabricate DPNs/MPC are obvious. First, the one-step synthesis is very easy and feasible. Second, it is a seed- and surfactant-free route, which is distinctly different from seed- and surfactant-directed strategies. Furthermore, notably, no functionalization process of MPC is needed, DPNs are directly grown on the surface of the MPC, promoting the better combination of two nanophases and preserving the intrinsic electronic structure of both DPNs and MPC. As-made DPNs/MPC nanocompsites exhibit high electrocatalytic activities toward oxidation of methanol and glucose.

2. Experimental section

2.1. Materials and chemicals

K_2PtCl_4 was obtained from Sinopharm Chemical Reagent Co., Ltd (Shanghai, China). HCOOH (98%), methanol and glucose were used as received from Beijing Chemical Reagent Company (Beijing, China). Commercial Pt/C catalyst was purchased from Alfa Aesar. Water used throughout all experiments was purified with the Millipore system.

2.2. Synthesis of DPNs/MPC

The MPC was prepared as previously reported.[25b] To synthesis of DPNs/MPC, 6 mg MPC were ultrasonically dispersed in a solution containing 2.04 ml K_2PtCl_4 aqueous solution (20 mM) and 3 ml HCOOH. This reaction solution was mildly sonicated for 30 min, and then placed at room temperature for 3 days. The product was collected by centrifugation, washed with water followed by ethanol for several times, and then dried in an oven at 60 ^oC for 5 h.

By varying of the used K_2PtCl_4 precursor amount to less (1.03 ml) and higher (6.15 ml), DPNs/MPC with different DPNs on MPC loading amount could be tuned.

The product prepared from 1.03, 2.04 and 6.15 ml of K_2PtCl_4 precursor (20 mM) were denoted as DPNs/MPC-1, DPNs/MPC-2, DPNs/MPC-3, respectively.

2.3. Characterizations

The morphologies and structures were characterized by a HITACHIH-8100 EM transmission electron microscope (TEM) with an accelerating voltage of 100 kV, and a JEM-2100F high-resolution transmission electron microscope (HRTEM) operating at 200 kV. XRD patterns were recorded on a D8 ADVANCE (Germany)

diffractometer equipped with Cu K (1.5406 Å) radiation. XPS measurement was performed on an ESCALAB-MKII spectrometer (VG Co. United Kingdom) with Al Kα X-ray radiation for excitation. Electrochemical experiments were carried out with a CHI 842c electrochemical analyzer (Chenhua Co., Shanghai, China). A conventional three electrode cell was used, including a platinum wire as counter electrode, a Ag/AgCl (saturated KCl) electrode as reference electrode and a modified glassy carbon electrode (GCE, 3 mm in diameter) as working electrode.

2.4. Electrochemical Investigations

Prior to the surface coating, the GC electrode was polished carefully with 1.0, and 0.05 μm alumina powder and rinsed with deionized water, followed by sonication in distilled water for a few minutes. Then, the electrode was allowed to dry under nitrogen. The catalyst dispersion was prepared by mixing 2 mg of catalyst in 0.1 mL Nafion (5 wt%) and 0.9 mL distilled water followed by ultrasonication for 30 min. After dropping 3.0 μL well-dispersed catalyst suspension onto the electrode surface, the electrode was dried at room temperature. Before the electrochemical test, the working electrode was first cycled for 100 cycles (-0.2 V to 1.2 V at 500 mV s^{-1}) in a N_2 saturated 0.5 M H_2SO_4 solution to generate clean electrode surface. Methanol electrocatalytic oxidation investigations were carried out in a 0.5 M H_2SO_4 solution containing 1 M methanol at a scan rate of 50 mV s^{-1}. Glucose electrocatalytic oxidation investigations were performed in 0.1 M phosphate buffered saline (PBS, pH=7.4) solution as a supporting electrolyte.

3. Results and Discussion

The morphology and structure of the products were investigated by transmission electron microscope (TEM). Fig. 1A showed the overall morphology of the pristine MPC. The pores of the MPC were uniform, close-packed and well-interconnected with a diameter of approximately 110 nm. In our synthesis, the morphology and loading density of the DPNs on MPC were controllable via simply varying of the used K_2PtCl_4 precursor amount, while the amount of MPC and HCOOH were fixed (Fig. 1B-D). Because of its high pore accessibility, the reactants fully accessed MPC, favoring the deposition of Pt nanostructures onto both inside and outside walls of the pore structure of the MPC. Kinetically, Pt nanonuclei were formed at the first stage though the reduction of K_2PtCl_4 by HCOOH, and then they aggregated to form discrete Pt nanoparticles. Due to the extremely slow reduction rate of K_2PtCl_4 by HCOOH, the discrete Pt nanoparticles were favorable for anisotropic overgrowth, preferentially in the <111> direction, according to the Lowest Energy principle,[15,26] thus leading to the formation of the DPNs. It is noted that in a low amount of Pt precursor (1.03 ml of 20 mM), irregular bumped nanoparticles were obtained on MPC (denoted as DPNs/MPC-1, Fig. 1B). With increasing Pt precursor (20 mM) amount to 2.04 ml, DPNs with highly branched arms were successfully formed (denoted as DPNs/MPC-2, Fig. 1C). The DNPs' sizes were roughly distributed from 20 to 80 nm with a dominating size of 40 nm. Further increasing of Pt precursor (20 mM) amount to 6.15 ml, DPNs densely covered on the whole surface of the MPC (denoted as DPNs/MPC-3, Fig. 1D), and the DPNs had a similar size distribution to that of DPNs/MPC-2. Therefore, in the present synthetic system, Pt precursor amount

was a key factor for the high-quality formation of the DPNs on MPC, which affected the Pt nucleation and crystal growth. Lower amount of K_2PtCl_4 precursor (1.03 ml of 20 mM K_2PtCl_4) led to insufficient Pt atoms to construct DPNs, resulting in irregular bumped Pt nanoparticles. Higher K_2PtCl_4 precursor amount (2.04 ml of 20 mM K_2PtCl_4) provided adequate Pt monomers for epitaxial growth, favoring the high quality formation of DPNs. While further increasing K_2PtCl_4 precursor amount (6.15 ml of 20 mM K_2PtCl_4), DPNs with aggregated form was appeared. Such a facile control of the morphology and loading density of DPNs on MPC was quite important for tuning their electrochemical properties.

The high-resolution TEM (HRTEM) image of individual DPN in DPNs/MPC-2 (Fig. 2A) showed a dendritic entity with branched arms in various directions. The highly ordered continuous fringe pattern of the core and the surrounding branches demonstrated a single-crystal structure, growing along the <111> direction, most likely, formic acid molecules played structure-directing role with its carboxyl group. Fig. 2B displayed a HRTEM image recorded from the edge of the DPNs, indicating that the diameter and length of the Pt branch were about 5 nm and 3-20 nm, respectively. Fig. 2C showed a highly magnified image of a single Pt branch with a *d* spacing of {111} plane of 0.23 nm. The inset in Fig. 2C was a fast Fourier transform (FFT) pattern recorded on the portion in the white square, which further confirmed the single crystal nature of the DPN. Selected area electron diffraction (SAED, Fig. 2D) pattern recorded on the area of Fig. 1C revealed a typical face centered cubic (*fcc*) Pt crystal structure similar to the bulk Pt.[15] The wide angle X-ray diffraction (XRD) pattern recorded on DPNs/MPC-2 (Fig. 3) confirmed a typical Pt *fcc* features, which

was consistent with the SAED investigation. The wide peak located at 23° was attributed to the MPC supporter. The other diffraction peaks were assigned to the characteristic (111), (200), (220), (311) and (222) planes of *fcc* Pt structure, respectively.

To gain insight on the chemical state of Pt in the DPNs/MPC-2 sample, the X-Ray photoelectron spectroscopy (XPS) was employed for the further investigation. Fig. 4A demonstrated significant Pt4f signals corresponding to the binding energy of Pt, which further confirmed the DPNs were successfully assembled on the MPC surface. The Pt4f spectrum divided into asymmetric doublet peaks centered at 71.15 and 74.50 eV (Fig. 4B), corresponding to the binding energies of Pt 4f7/2 and Pt 4f5/2 of metallic Pt^0,[27] respectively. Besides, no obvious shoulder peaks were observed at the higher binding energies, which represented Pt^{2+} and Pt^{4+} forms. These results fully indicated that the DPNs grown on the MPC were pure metallic Pt.

Unsupported DPNs with similar structures have been reported in recent pioneer studies.[12, 13] For instance, DPNs were synthesized by a two-step seeded growth route using preformed Pt seeds in the presence of poly(vinylpyrrolidone) via boiling refluxing of reaction solution.[12] In the reported synthetic strategies, the formations of DPNs were highly dependent on the selected seeds and surfactants to direct the dendritic growth of Pt nanoparticles. Notably, the proposed one-step, seed- and surfactant-free synthesis was quite different from the previous studies in its simplicity and feasibility. Furthermore, as-made DPNs/MPC had “clean” surfaces of both DPNs and MPC due to the surfactant- and surface functionalization-free synthetic process, ensuring to exhibit its intrinsic electrochemical activities.

Inspired by their attractive multimodal porous nanoarchitectures, the DPNs/MPC nanocompsites were explored as electrocatalysts for methanol oxidation reaction (MOR). Their electrocatalytic activities were benchmarked against commercial Pt/C catalyst. Fig. 5A presented the cyclic voltammograms (CVs) of DPNs/MPC-1, DPNs/MPC-2, DPNs/MPC-3 hybrids and commercial Pt/C catalysts (CPC), which were tested in 0.5 M H_2SO_4 containing 1 M methanol solution. Notably, the peak current density of the DPNs/MPC-2 (0.30 A mg^{-1}) in the positive direction sweep was higher than those of DPNs/MPC-1 (0.28 A mg^{-1}), DPNs/MPC-3 (0.08A mg^{-1}) and CPC (0.03 A mg^{-1}), respectively. It was noteworthy that the electrocatalytic activities of the DPNs/MPC nanocompsites were not proportionally increased with the Pt loading densities, due to the undesirable aggregation of DPNs on MPC. In a high density (DPNs/MPC-3), the DPNs overlapped each other on the MPC, leading to the loss of Pt active sites. Spatially and locally separated DPNs on MPC (DPNs/MPC-1 and DPNs/MPC-2) favored for the tolerance to susceptible DPNs aggregation on MPC, resulting in enhanced electrocatalytic activities in comparison with DPNs/MPC-3. The mass specific activity of the DPNs/MPC-2 was also higher than the reported supported Pt nanocomposites, such as Pt/N-doped carbon,[28] Pt/Sn/CNTs,[29] PtRuSnOx/CNTs,[30], Pt/polymeric ionic liquid microshere,[31] and Pt/hollow carbon spheres.[32] Furthermore, the onset potential for MOR on the DPNs/MPC-2 was negatively shifted about 200 mV compared with that of CPC, implying that MOR was more easily triggered at a lower potential on DPNs/MPC-2 in comparison with CPC.

Chronoamperometric curves recorded at 0.6 V for 2000 s (Fig. 5B), indicated

that DPNs/MPC-2 showed a higher initial current and limiting current density compared with reference samples, which were well in agreement with the CVs data. The rapid decay in the oxidation current density raised from the formation of intermediate and poisoning species, such as CO_{ads} during the oxidation of methanol.[33] Thus, all of the above data demonstrated that the DPNs/MPC could be considered as a promising nanoelectrocatalyst for MOR application.

The Pt/C hybrids are attracting electrochemical platform for electrocatalytic oxidation of glucose. The electrocatalytic performance of the as-prepared DPNs/MPC nanocomposites for glucose oxidation reaction was tested. Fig. 6A-B displayed the CVs of DPNs/MPC nanocomposites in the absence and presence of 50 mM glucose in a degassed 0.1 M phosphate buffered saline (PBS, pH=7.4) solution at a scan rate of 50 mV s^{-1}. In the absence of glucose, the voltammetric behavior of DPNs/MPC nanocomposites in the PBS were typical Pt feature with characteristic hydrogen adsorption/desorption peaks and Pt oxide/reduction peaks (Fig. 6A). In the presence of glucose, multiple anodic current peaks were clearly observed in the positive direction sweep (Fig. 6B), attributed to the oxidation of glucose together with resulted absorbed intermediates (at around 0.2 V) as well as Pt oxides.[34] In the negative direction sweep, with the reduction of surface Pt oxide, free Pt active sites were renewed and activated for the oxidation of glucose. Therefore, the glucose electro-oxidation current highly increased during the negative scan, forming a large and broad current peak in the potential range from 0.1 to -0.5 V. Compared with DPNs/MPC-1 and DPNs/MPC-3, DPNs/MPC-2 showed higher catalytic activity toward glucose oxidation. The mass normalized current density of DPNs/MPC-2

(0.024 A mg^{-1} at 0.06V) in the negative direction sweep was about 1.3 and 2.2 times higher than those of DPNs/MPC-1 (0.019 A mg^{-1} at 0.01V) and DPNs/MPC-3 (0.011 A mg^{-1} at 0.04 V), respectively.

Both CV and amperometric techniques were further employed to investigate the electrocatalytic activity of the DPNs/MPC-2 toward glucose oxidation by varying the glucose concentration. With increasing the glucose concentrations, the glucose oxidation current densities proportionately increased (Fig. 6C), while the oxidation potential slightly shifted positively (Fig. 6D). Fig. 7A displayed a typical amperometric response of the DPNs/MPC-2 on successive addition of glucose into stirring N_2-saturated PBS (0.1 M, pH=7.4) at an applied potential of 0.6 V. The DPNs/MPC-2 rapidly responded to the added glucose and achieved steady state current within 5 s (inset in Fig. 7A). Such a rapid response was quicker than those of Pt NPs/CNTs (11s),[35] PtPb nanowire (10 s),[36] and Pt nanoparticles/mesoporous carbon (10s).[37] Considering DPNs/MPC-2 with both porous DPNs and MPC, the enhanced electrocatalytic activity of the DPNs/MPC-2 might be caused by its sufficient active sites of Pt and favorable diffusion pathways in both DPNs and MPC for the rapid diffusion of glucose. A good linear relationship was realized between the oxidation peak current of glucose and its concentration in the range of 1-12 mM, with a detection limit of 0.13 mM based on S/N=3 (Fig. 7B). Therefore, as-prepared DPNs/MPC nanocomposite was a promising electrocatalytic platform for glucose oxidation reaction.

4. Conclusion

In summary, a one-step synthesis is proposed to directly fabricate newly

designed DPNs/MPC in aqueous solution at room temperature. The proposed strategy is unique in its seed- and surfactant-free design, making it quite different from tow-step seed-directed and surfactant-mediated strategies to formation DPNs. Furthermore, original MPC is directly used without the need for any surface functionalization (e.g., amino-functionalized process), making the synthesis as simple and feasible as possible. As-prepared DPNs/MPC with ‘‘clean’’ surfaces of both DPNs and MPC as well as spatially and locally separated DPNs on MPC shows high electrocatalytic activities toward oxidation of methanol and glucose.

Acknowledgements

This work was supported by National Natural Science Foundation of China (No. 21273218).

References

1. (a) S. Guo and E. Wang, *Nano Today*, 2011, **6**, 240-264. (b) C. Li, H. Wang and Y. Yamauchi, *Chem.-Eur. J.*, 2013, **19**, 2242-2246. (c) Y. Yamauchi, *J. Ceram. Soc. Jpn.*, 2013, **121**, 831-840. (d) H. Wang and Y. Yamauchi, *Chem.-Asian J.*, 2012, **7**, 2133-2138.
2. C. Chen and P. Holt-Hindle, *Chem. Rev.*, 2010, **110**, 3767-3804.
3. A. Ciszewski and G. Milczarek, *Anal. Chem.*, 1999, **71**, 1055-1061.
4. C. Sun, H. Lee, J. Yang and C. Wu, *Biosens. Bioelectron.*, 2011, **26**, 3450-3455.
5. R. Polsky, R. Gill, L. Kaganovsky and I. Willner, *Anal. Chem.*, 2006, **78**, 2268-2271.
6. J. Yuan, K. Wang and X. Xia, *Adv. Funct. Mater.*, 2005, **15**, 803-809.
7. S. Park, T. D. Chung and H. C. Kim, *Anal. Chem.*, 2003, **75**, 3046-3049.
8. S. Guo, D. Wen, Y. Zhai, S. Dong and E. Wang, *ACS Nano*, 2010, **4**, 3959-3968.
9. N. C. Bigall, T. Härtling, M. Klose, P. Simon, L. M. Eng and A. Eychmüller, *Nano Lett.*, 2008, **8**, 4588-4592.
10. Y. Song, W. A. Steen, D. Peña, Y. Jiang, C. J. Medforth, Q. Huo, J. L. Pincus, Y. Qiu, D. Y. Sasaki and J. E. Miller, *Chem. Mater.*, 2006, **18**, 2335-2346.
11. Y. Song, Y. Yang, C. J. Medforth, E. Pereira, A. K. Singh, H. Xu, Y. Jiang, C. J. Brinker, F. van Swol and J. A. Shelnutt, *J. Am. Chem. Soc.*, 2004, **126**, 635-645.
12. M. A. Mahmoud, C. E. Tabor, M. A. El-Sayed, Y. Ding and Z. L. Wang, *J. Am. Chem. Soc.*, 2008, **130**, 4590-4591.
13. L. Wang and Y. Yamauchi, *J. Am. Chem. Soc.*, 2009, **131**, 9152-9153.
14. Y. Xia, H. B. Wu, X. Wang and X. W. D. Lou, *Angew. Chem., Int. Ed.*, 2013, **52**,

12337-12340.

15. J. Chen, T. Herricks, M. Geissler and Y. Xia, *J. Am. Chem. Soc.*, 2004, **126**, 10854-10855.
16. Y. Yamauchi, A. Takai, T. Nagaura, S. Inoue and K. Kuroda, *J. Am. Chem. Soc.*, 2008, **130**, 5426-5427.
17. S. Sun, D. Yang, D. Villers, G. Zhang, E. Sacher and J.-P. Dodelet, *Adv. Mater.*, 2008, **20**, 571-574.
18. S. Sun, F. Jaouen and J. P. Dodelet, *Adv. Mater.*, 2008, **20**, 3900-3904.
19. Z. Liu, X. Lin, J. Y. Lee, W. Zhang, M. Han and L. M. Gan, *Langmuir*, 2002, **18**, 4054-4060.
20. S. Sharma, A. Ganguly, P. Papakonstantinou, X. Miao, M. Li, J. L. Hutchison, M. Delichatsios and S. Ukleja, *J. Phys. Chem. C*, 2010, **114**, 19459-19466.
21. X. Bo, L. Zhu, G. Wang and L. Guo, *J. Mater. Chem.*, 2012, **22**, 5758-5763.
22. R. Balgis, S. Sago, G. M. Anilkumar, T. Ogi and K. Okuyama, *ACS Appl. Mater. Interfaces*, 2013, **5**, 11944-11950.
23. J. Yu, S. Kang, S. B. Yoon and G. Chai, *J. Am. Chem. Soc.*, 2002, **124**, 9382-9383.
24. X. Bo and L. Guo, *Electrochim. Acta*, 2013, **90**, 283-290.
25. (a) Y. Zhang, X. Bo, C. Luhana, H. Wang, M. Li, L. Guo. *Chem. Commun.*, 2013, **49**, 6885-6887. (b) M. Zhou, L. Shang, B. Li, L. Huang and S. Dong, *Biosens. Bioelectron.*, 2008, **24**, 442-447. (c) M. Zhou, L. Shang, B. Li, L. Huang and S. Dong, Electrochem. Commun., 2008, **10**, 859–863.
26. S. Sun, G. Zhang, D. Geng, Y. Chen, R. Li, M. Cai and X. Sun, *Angew. Chem.*,

Int. Ed., 2011, **123**, 442-446.

27. S. Guo, S. Dong and E. Wang, *ACS Nano*, 2009, **4**, 547-555.
28. Pan, L. Qiu, Y. Peng and F. Yan, *J. Mater. Chem.*, 2012, **22**, 13578-13584.
29. S. Sun, G. Zhang, D. Geng, Y. Chen, M. N. Banis, R. Li, M. Cai and X. Sun, *Chem. Eur. J.*, 2010, **16**, 829-835.
30. T. Huang, R. Jiang, J. Liu, J. Zhuang, W. Cai and A. Yu, *Electrochim. Acta*, 2009, **54**, 4436-4440.
31. J. Yang, L. Qiu, B. Liu, Y. Peng, F. Yan and S. Shang, *J. Polym. Sci., Part A: Polym. Chem.*, 2011, **49**, 4531-4538.
32. Z. Wen, Q. Wang, Q. Zhang and J. Li, *Electrochem. Commun.*, 2007, **9**, 1867-1872.
33. T. Ralph and M. Hogarth, *Platin. Met. Rev.*, 2002, **46**, 117-135.
34. J. Wang, D. F. Thomas and A. Chen, *Anal. Chemistry.*, 2008, **80**, 997-1004.
35. D. Rathod, C. Dickinson, D. Egan and E. Dempsey, *Sens. Actuators B, Chem.*, 2010, **143**, 547-554.
36. Y. Bai, Y. Sun and C. Sun, *Biosens. Bioelectron.*, 2008, **24**, 579-585.
37. C. Su, C. Zhang, G. Lu and C. Ma, *Electroanal.*, 2010, **22**, 1901-1905.

Figures and Figure Captions

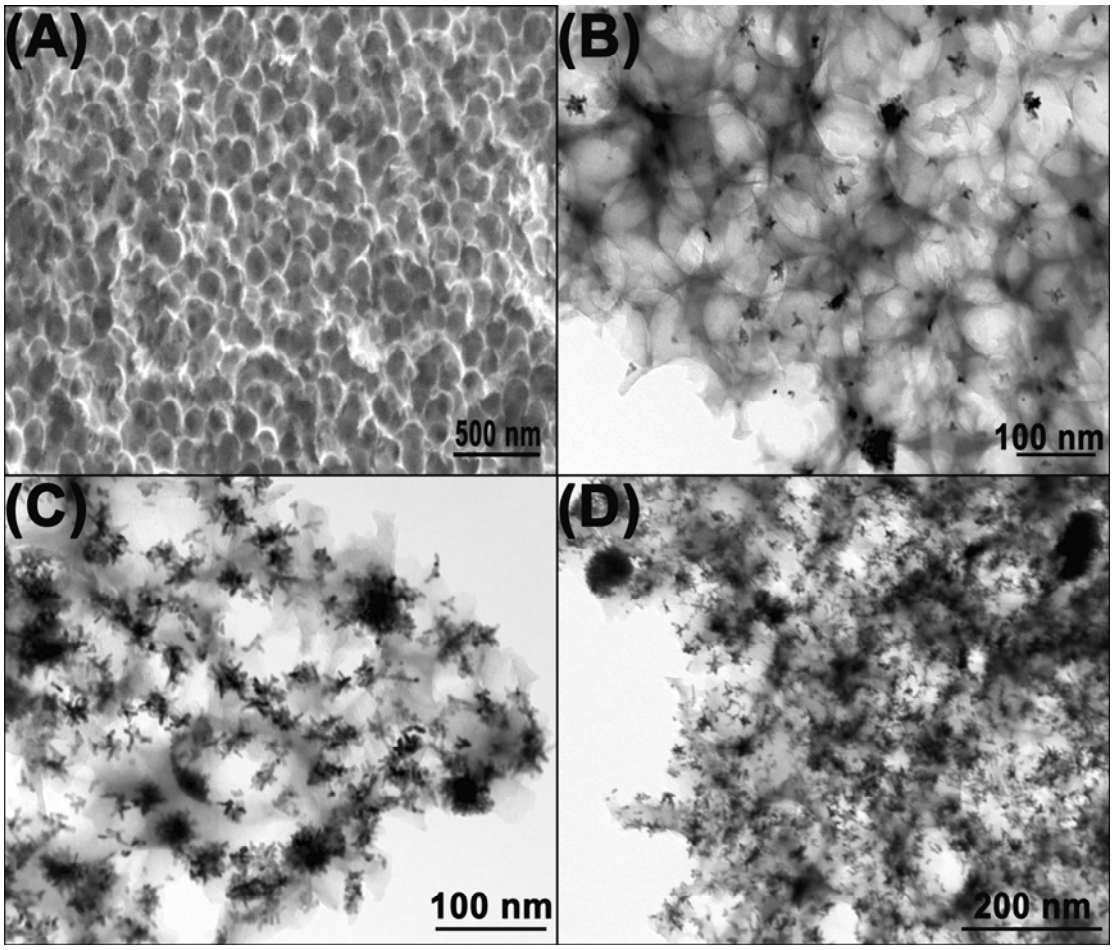

Fig. 1 TEM images of (A) bare MPC, (B) DPNs/MPC-1, (C) DPNs/MPC-2 and (D) DPNs/MPC-3.

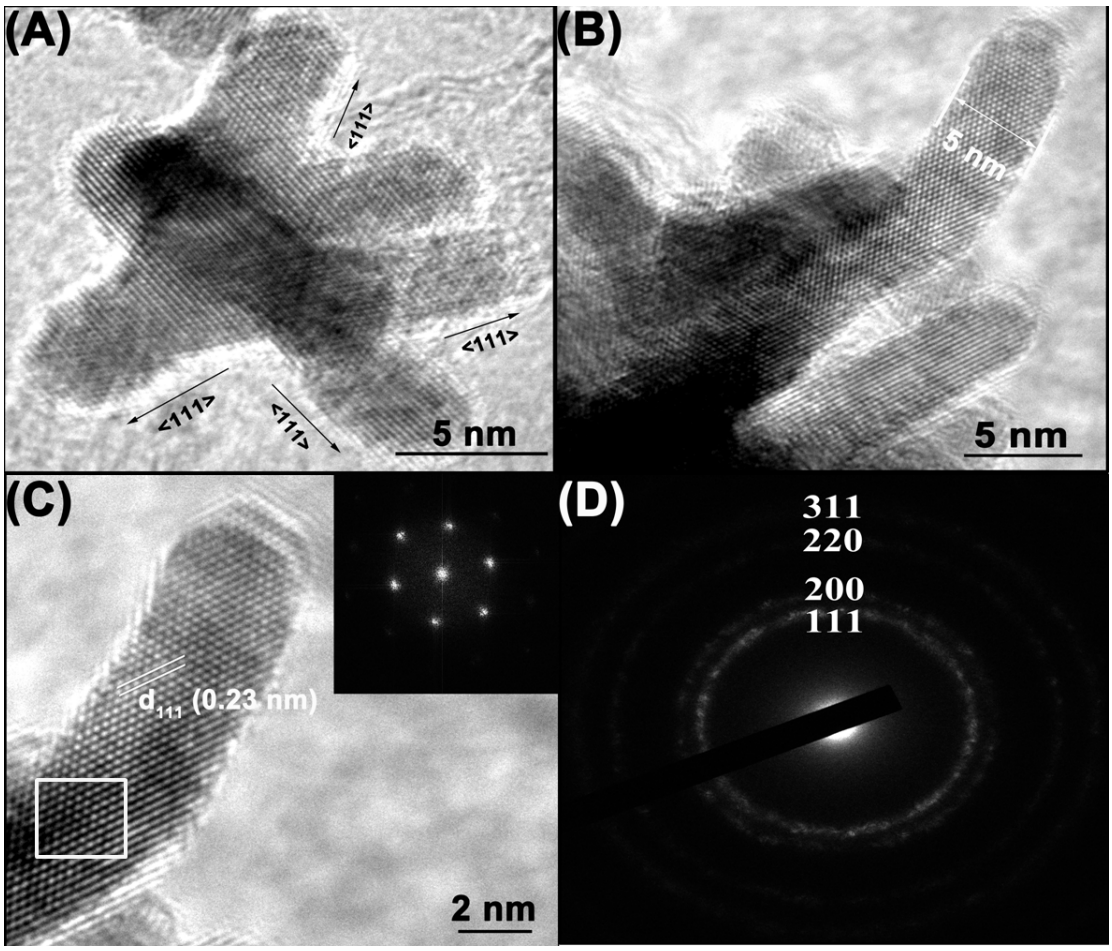

Fig. 2 (A) HRTEM image of one DPN grown on MPC. The highly ordered continuous fringe patterns of the overall DPN demonstrate a single-crystal structure, growing along the {111} direction. (B) HRTEM image of the edge of DPN. (C) Enlarged HRTEM image of a single Pt branch, with a FFT pattern in the inset recorded on the portion in the white square. (D) Selected area electron diffraction pattern of DPNs.

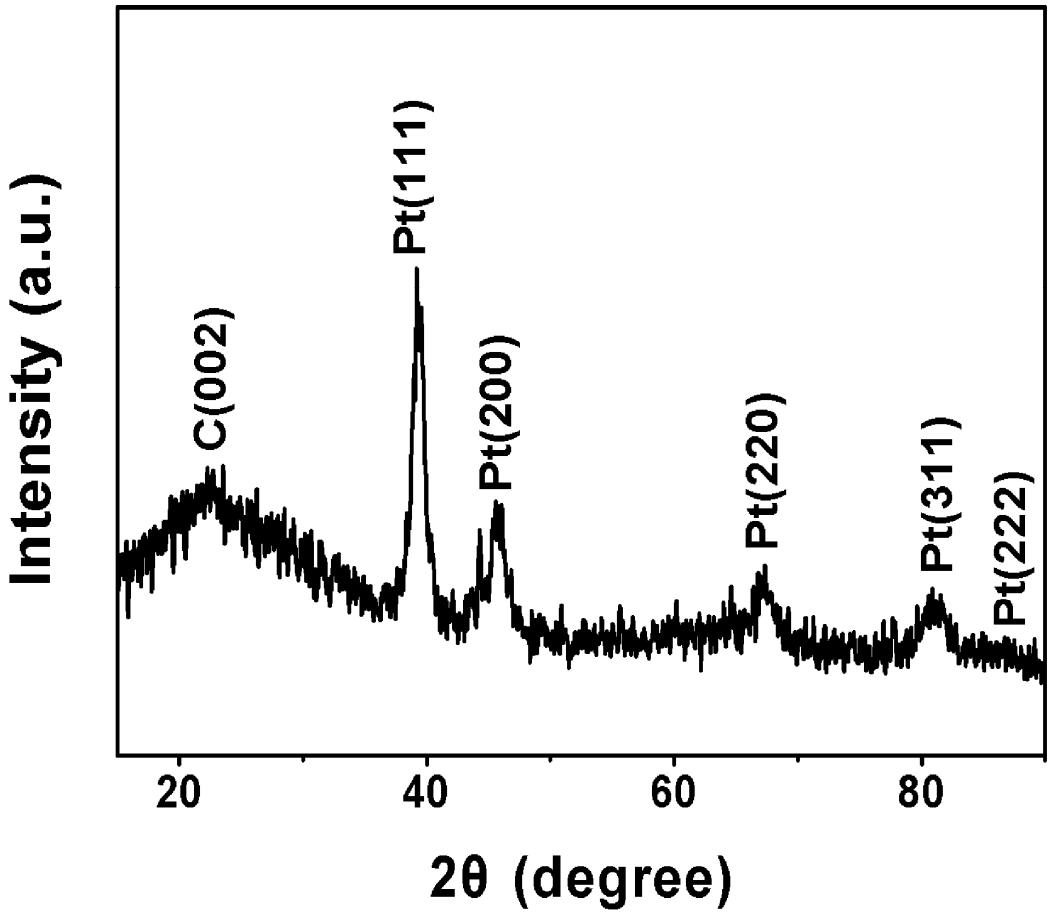

Fig. 3 XRD pattern of the DPNs/MPC-2 hybrid. The C peak is from the MPC.

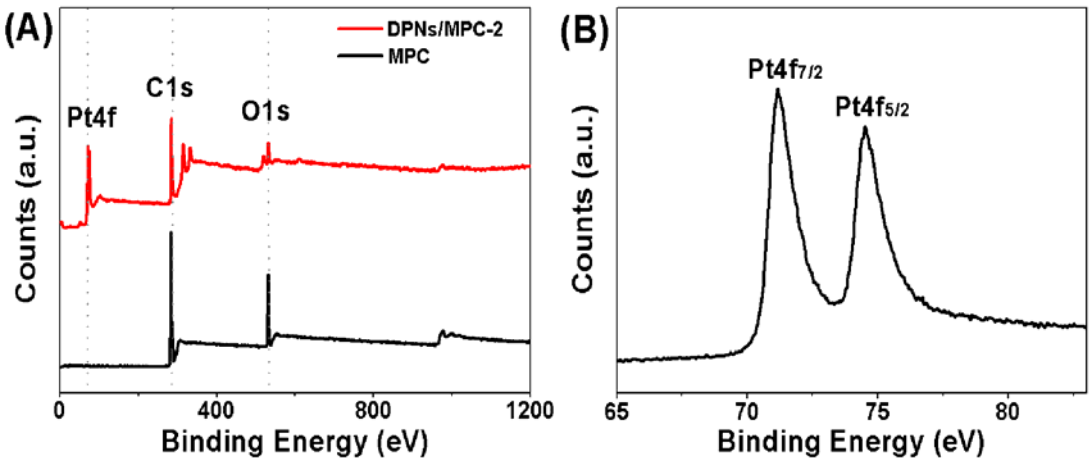

Fig. 4 (A) Typical XPS spectra of MPC before (black line) and after DPNs deposition (red line). (B) XPS pattern of Pt4f.

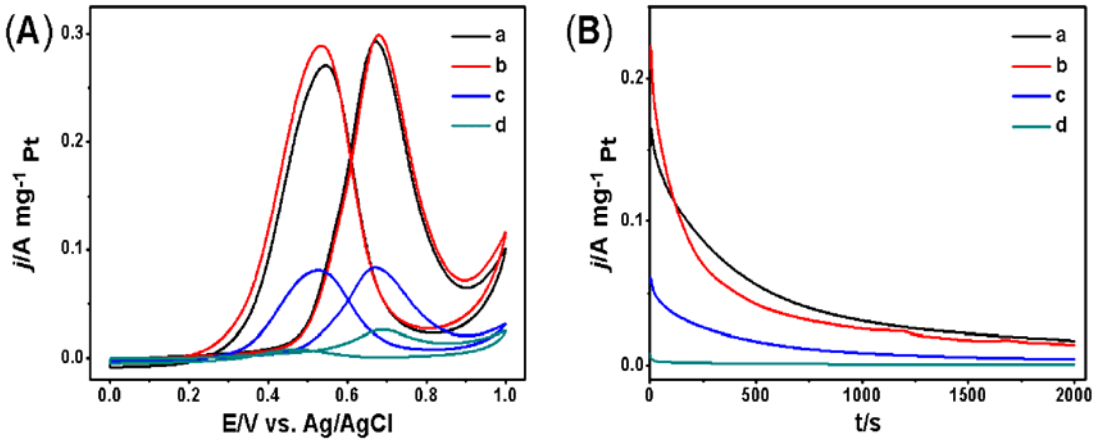

Fig. 5 (A) Cyclic voltammograms and (B) chronoamperometric curves of MOR catalyzed by DPNs/MPC-1 (a), DPNs/MPC-2 (b), DPNs/MPC-3 (c) and commercial Pt/C catalyst (d), respectively, in degassed 0.5 M H_2SO_4 solution containing 1 M methanol. The chronoamperometric curves were recorded at 0.6 V.

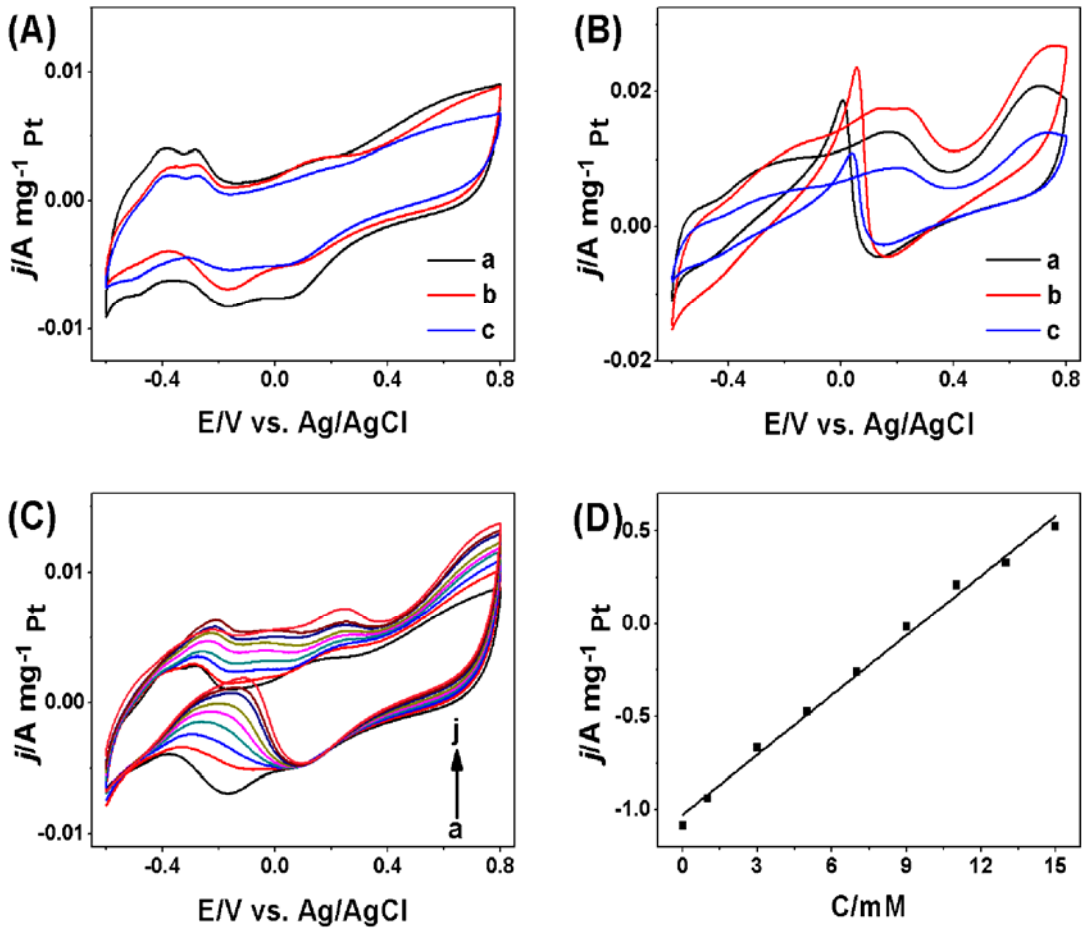

Fig. 6 CVs of DPNs/MPC-1 (a), DPNs/MPC-2 (b) and DPNs/MPC-3 (c) in 0.1 M PBS in the absence (A) and presence (B) of 50 mM glucose at a scan rate of 50 mV s^{-1}, respectively. (C) CVs of glucose oxidation catalyzed by DPNs/MPC-2 in 0.1 M PBS (PH=7.4) in the presence of glucose with different concentrations (from bottom to top): (a) 0, (b) 1, (c) 3, (d) 5, (e) 7, (f) 9, (h) 11, (i) 13, and (j) 15 mM. (D) The corresponding calibration plot for glucose detection.

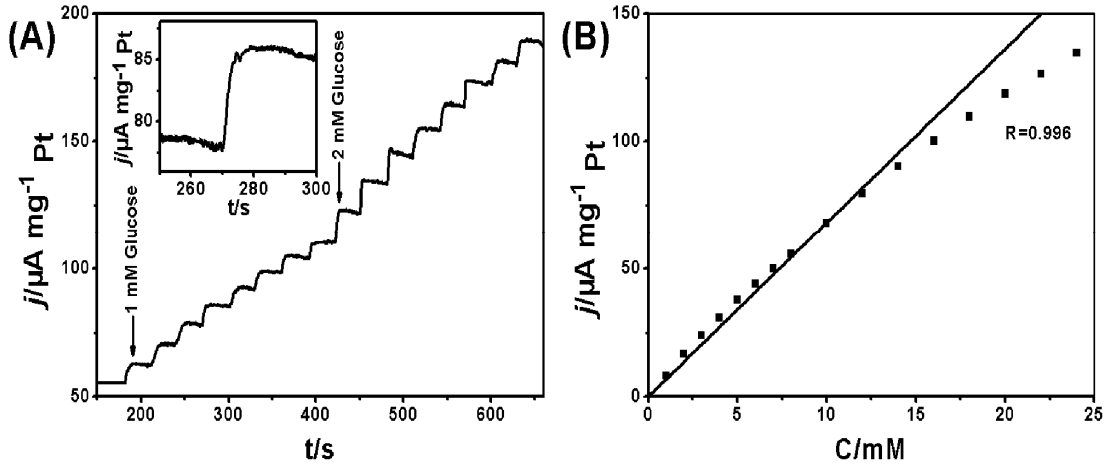

Fig. 7 (A) Chronoamperometric curves of DPNs/MPC-2 modified GC electrode with successive addition glucose into stirring N_2-saturated PBS (0.1 M, pH=7.4) at an applied potential of 0.6 V. Inset shows the current response time caused by 1 mM glucose. (B) The corresponding calibration plot for the oxidation of glucose at 0.6 V.

Graphical Abstract

Dendritic platinum nanoparticles decorated macroporous carbon, a promising electrocatalyst, is fabricated by a one-step synthesis.